JOC Featured Article

pubs.acs.org/joc

N-Acetyl Side-Chains in Saccharides: NMR *J*-Coupling Equations Sensitive to CH−NH and NH−CO Bond Conformations in 2-Acetamido-2-deoxy-aldohexopyranosyl Rings

Xiaosong Hu,[†] Ian Carmichael,[‡] and Anthony S. Serianni*,[†]

[†]*Department of Chemistry and Biochemistry and* [‡]*Radiation Laboratory, University of Notre Dame, Notre Dame, Indiana 46556*

aseriann@nd.edu

Received March 23, 2010

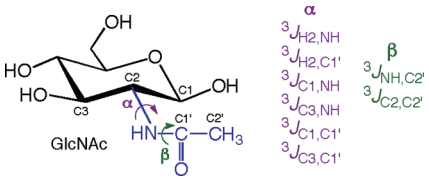

Eight Karplus relationships have been determined for use in conformational studies of saccharide *N*-acetyl side-chains in solution by NMR spectroscopy. Density functional theory was used to calculate $^{1}H-^{1}H$, $^{13}C-^{1}H$, and $^{13}C-^{13}C$ NMR spin-coupling constants in four model compounds that mimic α-*gluco*, *β-gluco*, α-*allo*, and *β-allo* 2-acetamido-2-deoxy-D-aldohexopyranosyl ring configurations in order to study the effects of C1 and C3 configuration adjacent to the *N*-acetyl group on coupling behavior. Six vicinal *J*-couplings sensitive to the C2−N2 torsion angle were parametrized: $^{3}J_{H2,NH}$, $^{3}J_{H2,CO}$, $^{3}J_{C1,NH}$, $^{3}J_{C3,NH}$, $^{3}J_{C1,CO}$ and $^{3}J_{C3,CO}$. Two vicinal *J*-couplings sensitive to amide bond conformation (*cis* and *trans* amide) were also investigated, namely, $^{3}J_{NH,\underline{C}H_3}$ and $^{3}J_{C2,\underline{C}H_3}$. In relevant cases, comparisons were made to analogous coupling pathways found in proteins to evaluate the effects of peptide versus saccharide pathway structure on coupling magnitude. These parametrizations allow multiple, redundant *J*-couplings within the *N*-acetyl fragment of saccharides and related structures to be used for more confident assignments of side-chain conformation in biologically important saccharides, especially those where this structural element may play a role in molecular recognition or other biological processes. This application is illustrated in an analysis of experimental *J*-couplings measured within the *N*-acetyl side-chain of a ^{13}C-labeled methyl *N*-acetyl-α-D-glucosaminide.

Introduction

The universal language adopted by complex carbohydrates to communicate information in biological systems remains largely elusive.[1] Unlike proteins and nucleic acids, whose primary structures are tightly linked through the processes of transcription and translation, the introduction of saccharides into complex structures such as proteins appears, at current levels of understanding, less organized and predictable, leading to an inability to articulate a tidy universal code underlying the carbohydrate language. It is possible that a subtle form of chemical communication is involved, such as the ordering of solvent water or ions at molecular interfaces involving saccharides, which through unknown mechanisms translates into specific cellular signals that enable specific biofunctions.[2]

In recent years, it has become evident that changes in side-chain structure can result in significant structural perturbations in saccharides, some of which may exert important chemical and biological effects.[3] Side-chain structure modulates overall saccharide ring structure and thus reactivity, and arguably equal attention should be paid to these appendages as to the carbon scaffolds supporting them. Underlying this assertion is the fact that, for the most part, saccharides

(1) (a) *Essentials of Glycobiology*; Varki, A., Cummings, R., Esko, J. D., Freeze, H., Hart, G. W., Marth, J., Eds.; Cold Spring Harbor Lab Press: Cold Spring Harbor, NY, 1999. (b) Pilobello, K. T.; Slawek, D. E.; Mahal, L. K. *Proc. Natl. Acad. Sci. U.S.A.* **2007**, *104*, 11534–11539.

(2) (a) Fryer, H. J. L.; Hockfield, S. *Curr. Opin. Neurobiol.* **1996**, *6*, 113–118. (b) Heyden, M.; Bründermann, E.; Heugen, U.; Niehues, G.; Leitner, D. M.; Havenith, M. *J. Am. Chem. Soc.* **2008**, *130*, 5773–5779. (c) Eriksson, M.; Lindhorst, T. K.; Hartke, B. *J. Chem. Phys.* **2008**, *128*, 105105.

(3) (a) Serianni, A. S.; Wu, J.; Carmichael, I. *J. Am. Chem. Soc.* **1995**, *117*, 8645–8650. (b) Cloran, F.; Zhu, Y.; Osborn, J.; Carmichael, I.; Serianni, A. S. *J. Am. Chem. Soc.* **2000**, *122*, 6435–6448. (c) Klepach, T.; Zhang, W.; Carmichael, I.; Serianni, A. S. *J. Org. Chem.* **2008**, *73*, 4376–4387.

DOI: 10.1021/jo100521g Published on Web 07/06/2010

SCHEME 1

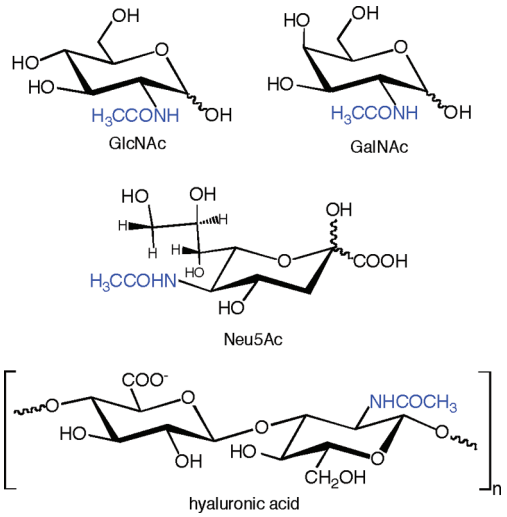

commonly contain a high density of exocyclic lone-pair electrons that are capable of interacting with the saccharide backbone in a manner that modulates the structure of the latter. This feature is unique among the various classes of biomolecules, thus leading to the speculation that these lone-pairs play an important and unique role in saccharide biocommunication. For these reasons, considerable effort has been devoted in this and other laboratories toward improving NMR-based methods to characterize important side-chain substituents such as hydroxyl and hydroxymethyl groups.[4]

In the present investigation, this line of inquiry is extended to *N*-acetyl side-chains, which are found in biologically important monosaccharides such as *N*-acetyl-D-glucosamine (GlcNAc), *N*-acetyl-D-galactosamine (GalNAc) and *N*-acetylneuraminic acid (Neu5Ac) (Scheme 1) and are constituents of the oligosaccharides of *O*- and *N*-linked glycoproteins.[5] The *N*-acetyl side-chain constituents of biopolymers such as hyaluronic acid (Scheme 1), contributed by GlcNAc residues, appear to play an important H-bonding role that dictates preferred conformation of the polymer in solution.[6] Recently, the thermodynamics and kinetics of amide *cis*–*trans* isomerization have been characterized in GlcNAc and related monosaccharides, demonstrating that this side-chain is not structurally homogeneous but that measurable amounts of both *cis* and *trans* amide conformations are present in aqueous solution.[7] Recent work has been reported on the synthesis of $^{13}C/^{15}N$ labeled 2-amino-2-deoxy-aldoses and their *N*-acetyl derivatives, and some *J*-couplings involving the carbons and hydrogens within the pyranosyl ring of these

SCHEME 2

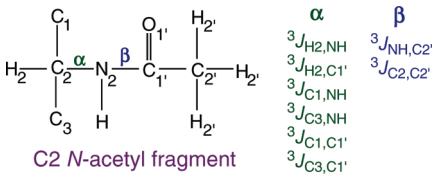

molecules have been studied.[8] ^{13}C-Labeling of the *N*-acetyl side-chain of Neu5Ac has been described recently in NMR studies of the sialyltransferase ST6-Gal-I.[9]

In the present work, NMR *J*-couplings involving the *N*-acetyl side-chain carbons and hydrogens of 2-acetamido-2-deoxy-aldopyranoses have been investigated. In addition to the $^3J_{H2,NH}$ spin-coupling constant commonly recognized as a means to evaluate conformation about the C2–N2 bond (defined herein as the α bond of the side-chain; Scheme 2) in solution,[10,11] five additional vicinal *J*-couplings sensitive to C2–N2 bond conformation provide structural information complementary to $^3J_{H2,NH}$ and have been investigated: $^3J_{H2,C1'}$, $^3J_{C1,NH}$, $^3J_{C3,NH}$, $^3J_{C1,C1'}$ and $^3J_{C3,C1'}$ (Scheme 2). The effects of configuration at C1 and C3 of the aldopyranosyl ring on these six spin-couplings were investigated using density functional theory (DFT) to compute *J*-couplings under *in vacuo* and solvated conditions. Two spin-couplings, $^3J_{NH,C2'}$ and $^3J_{C2,C2'}$, were also investigated as potential probes of *cis*/*trans* conformation of the amide bond (defined herein as the *β* bond of the side-chain; Scheme 2). Structural factors influencing the magnitudes of these eight vicinal *J*-couplings have been identified, and new parametrized equations correlating their magnitudes with molecular torsion angles in *N*-acetylated saccharides (and related structures containing this side-chain) have been derived to assist in structural interpretations of these *J*-couplings in solution.

Calculations

A. Energy Calculations. Two groups of model structures were used to calculate the effects of C2–N2 and N2–C1′ (amide) bond rotation (Scheme 2) on total energy using density functional theory (DFT) and the *Gaussian03*[12] suite of programs. *In vacuo* energy calculations were first performed using the B3LYP functional[13] and the 6-31G* basis set[14] on an unsubstituted *N*-acetylated cyclohexane model (**1**) (Scheme 3) to provide baseline behavior in a system devoid of proximal substituent effects. In these calculations (*Group 1A*), rotation about the amide bond, denoted *β* in the side-chain (Scheme 3) and formally defined as the C1–N1–C1′–C2′ torsion angle, was performed in 15° increments through the full 360° rotation, while conformation about the C1–N1 bond, denoted α (Scheme 3) and formally defined as the H1–C1–N1–H torsion angle, was confined to two limiting geometries, namely, α-*syn* (H1–C1–N1–H, C2–C1–N1–C1′ and C6–C1–N1–C1′ torsions fixed at 0°, −60° and 60°, respectively) and α-*anti* (H1–C1–N1–H, C2–C1–N1–C1′

(4) (a) Thibaudeau, C.; Stenutz, R.; Hertz, B.; Klepach, T.; Zhao, S.; Wu, Q.; Carmichael, I.; Serianni, A. S. *J. Am. Chem. Soc.* **2004**, *126*, 15668–15685. (b) Zhao, H.; Pan, Q.; Zhang, W.; Carmichael, I.; Serianni, A. S. *J. Org. Chem.* **2007**, *72*, 7071–7082.

(5) Arnold, J. N.; Wormald, M. R.; Sim, R. B.; Rudd, P. M.; Dwek, R. A. *Annu. Rev. Immunol.* **2007**, *25*, 21–50.

(6) (a) Napier, M. A.; Hadler, N. M. *Proc. Natl. Acad. Sci. U.S.A.* **1978**, *75*, 2261–2265. (b) Cowman, M. K.; Cozart, D.; Nakanishi, K.; Balazs, E. A. *Arch. Biochem. Biophys.* **1984**, *230*, 203–212. (c) Donati, A.; Magnani, A.; Bonechi, A.; Barbucci, R.; Rossi, C. *Biopolymers* **2001**, *59*, 434–445. (d) Almond, A.; Brass, A.; Sheehan, J. K. *Glycobiology* **1998**, *8*, 973–980. (e)

(7) Hu, X.; Zhang, W.; Carmichael, I.; Serianni, A. S. *J. Am. Chem. Soc.* **2010**, *132*, 4641–4652.

(8) Zhu, Y.; Pan, Q.; Thibaudeau, C; Zhao, S.; Carmichael, I.; Serianni, A. S. *J. Org. Chem.* **2006**, *71*, 466–479.

(9) Macnaughtan, M. A.; Tian, F.; Liu, S.; Meng, L.; Park, S.; Azadi, P.; Moremen, K. W.; Prestegard, J. H. *J. Am. Chem. Soc.* **2008**, *130*, 11864–11865.

(10) Holmbeck, S. M. A.; Petillo, P. A.; Lerner, L. E. *Biochemistry* **1994**, *33*, 14246–14255.

(11) Mobli, N.; Almond, A. *Org. Biomol. Chem.* **2007**, *5*, 2243–2251.

(12) Frisch, M. J., et al. *Gaussian03, Revision A.1*; Gaussian, Inc.: Pittsburgh, PA, 2003.

(13) Becke, A. D. *J. Chem. Phys.* **1993**, *98*, 5648–5652.

(14) Hehre, W. J.; Ditchfield, R.; Pople, J. A. *J. Chem. Phys.* **1972**, *56*, 2257–2261.

SCHEME 3

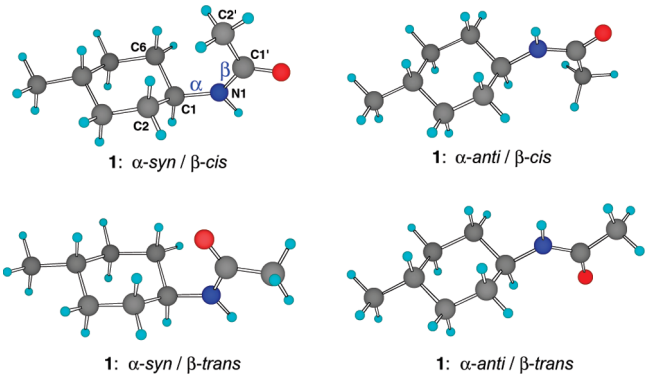

SCHEME 4

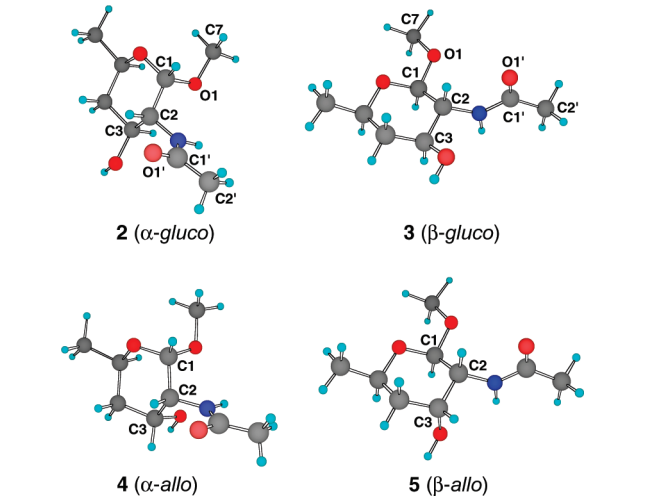

and C6−C1−N1−C1′ torsions fixed at 180°, 120° and −120°, respectively) (representative α and β geometries in **1** are shown in Scheme 3). A second set of calculations (*Group 1B*) was obtained on **1** in the same fashion, except that the effects of solvation by water were mimicked using the self-consistent reaction field (SCRF)[15] and the integral equation formalism (polarizable continuum) model (IEFPCM)[16] implemented in *Gaussian03*[12] (a dielectric of 78.39 was used in all solvated calculations in this work). The United Atom Topological Model (UAHF)[17] was applied in these calculations by setting RADII = UAHF in the input file to assist convergence during energy minimization.

In a second series of energy calculations, model structures **2**−**5** (Scheme 4) were employed that more closely mimic the methyl aldohexopyranosides of α- and β-GlcNAc and α- and β-AllNAc (*N*-acetyl-D-allosamine), since they bear an -OCH_3 substituent at C1 and an hydroxyl group at C3. In these *in vacuo* geometry calculations (*Group 2A*), the C2−N2−C1′−C2′ torsion angle (β) was rotated in 15° increments through 360° in two fixed geometries about α (for α-*syn*, the H2−C2−N2−H, C1−C2−N2−C1′ and C3−C2−N2−C1′ torsion angles were fixed at 0°, −60° and 60°, respectively; for α-*anti*, these torsions were fixed at 180°, 120° and −120°, respectively). In all calculations, the C2−C1−O1−C7 and C2−C3−O3−H torsion angles were fixed at 180°.

Model structures **2**−**5** were also used in a final set of *in vacuo* geometry calculations (*Group 2B*) in which the C1−C2−N2−C1′ torsion angle (α) was rotated in 15° increments through 360°. The H−N2−C1′−O1′ torsion angle was set initially at 0° (β-*cis*) or 180° (β-*trans*) but was allowed to relax during geometry optimization, and the exocyclic C2−C1−O1−C7 and C2−C3−O3−H torsion angles were fixed at 180°.

B. NMR *J*-Coupling Calculations. NMR spin−spin coupling constants were calculated using density functional theory (DFT) as implemented in *Gaussian03*.[12] The B3LYP functional was employed, and an extended basis set, a [5s2p1d|3s1p] contraction of a [9s5p1d|5s1p] set of Gaussian primitives, was used in all calculations, as discussed in previous publications.[18] Reported couplings are unscaled, include both Fermi and non-Fermi contact terms, and were calculated *in vacuo*. *In vacuo* optimized geometries in Groups 2A and 2B (see above) were used to parametrize equations for the following *J*-couplings: for α, $^3J_{H2,NH}$, $^3J_{H2,C1'}$, $^3J_{C1,NH}$, $^3J_{C3,NH}$, $^3J_{C1,C1'}$ and $^3J_{C3,C1'}$ (data from *Group 2A*); for β, $^3J_{NH,C2'}$ and $^3J_{C2,C2'}$ (data from *Group 2B*).

C. Effects of Solvation on Calculated Geometries and NMR *J*-Couplings. A limited set of calculations was generated to investigate the effects of solvent water in one or both components of the *J*-coupling calculations, namely, the optimized geometries employed in the calculations, and the *J*-coupling calculations themselves. This information was obtained on model **3** (β-*gluco*) only, with the assumption that its behavior will be representative of those for **2**, **4** and **5**. The solvation methodology employed was similar to that described for *Group 1B* above (*i.e.*, the self-consistent reaction field (SCRF) and the integral equation formalism (polarizable continuum) model (IEFPCM) were employed). The following combinations were investigated: $\text{geometries}_{vac}/J\text{-coupling}_{vac}$ (from *Group 2B*); $\text{geometries}_{sol}/J\text{-couplings}_{vac}$; $\text{geometries}_{vac}/J\text{-couplings}_{sol}$; $\text{geometries}_{sol}/J\text{-couplings}_{sol}$.

D. Equation Parametrization. Equations describing the dependencies of $^3J_{HH}$, $^3J_{CH}$ and $^3J_{CC}$ on molecular torsion angles were parametrized using the nonlinear curve-fitting module integrated in OriginPro[19] implemented on a desktop PC. Coefficients of the Fourier series used to formulate the equations were generated randomly, and for each set of coefficients, the deviations between couplings predicted by the fitted equation and those from the reference data set were calculated in the form of a χ^2 parameter (see more discussion in Supporting Information). Parameter values were then adjusted automatically to reduce the value of χ^2. When the difference in χ^2 values computed from two successive iterations was smaller than the set tolerance (1×10^{-9}), the fitting procedure was considered converged and further exploration of parameters was halted. The goodness-of-fit of each equation is reported as an rms value (see more discussion in Supporting Information).

Results and Discussion

A. Energetics: Cyclohexane Model 1. Rotation of the C1−N1−C1′−C2′ (amide; β) bond in **1** produced symmetric energy plots, with minima located at 0° (*cis*) and 180° (*trans*), and maxima located at 90° and −90° (Figure S1, Supporting Information). The activation barrier for interconversion of *cis* and *trans* amides ranged from 25.5 − 27.7 kcal/mol, and inclusion of solvent displaced both the α-*syn* and α-*anti* curves to lower energies while activation barriers remained essentially unchanged. Plots for the α-*syn* geometry were displaced to slightly higher energies (2−5 kcal) in both the *in vacuo* and solvated data sets. In all data sets, the *trans* amide was more stable than the *cis* amide, but the energy difference

(15) Cancés, M. T.; Mennucci, B.; Tomasi, J. *J. Chem. Phys.* **1997**, *107*, 3032–3037.
(16) Cammi, R.; Mennucci, B.; Tomasi, J. *J. Chem. Phys. A* **2000**, *104*, 5631–5637.
(17) Barone, V.; Cossi, M.; Tomasi, J. *J. Chem. Phys.* **1997**, *107*, 3210–3221.
(18) Stenutz, R.; Carmichael, I.; Widmalm, G.; Serianni, A. S. *J. Org. Chem.* **2002**, *67*, 949–958.
(19) *OriginPro 8*, v8.0725; OriginLab: Northampton, MA, 2007.

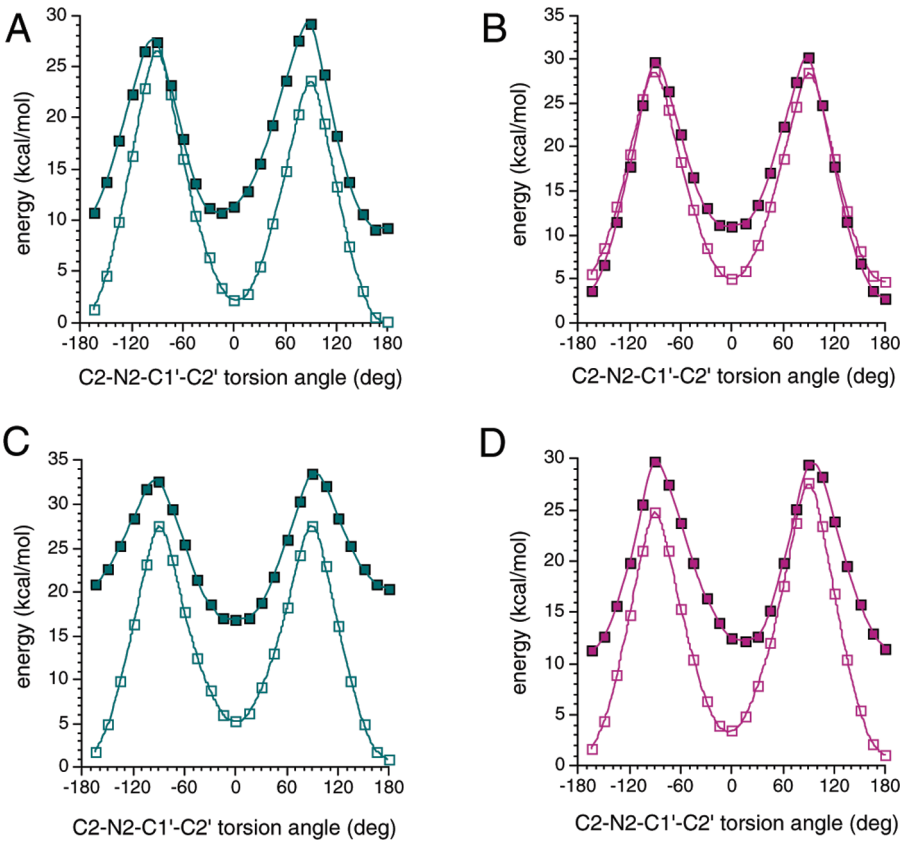

FIGURE 1. Effect of C2−N2−C1′−C2′ bond rotation on total energy in **2**−**5** (*in vacuo*). Filled symbols, α-*syn*; open symbols, α-*anti*. (A) α-*gluco* **2**. (B) β-*gluco* **3**. (C) α-*allo* **4**. (D) β-*allo* **5**.

in both the *in vacuo* and solvated data sets was larger for α-*syn* (∼5.8 kcal) than for α-*anti* (∼2.6 kcal).

B. Energetics: Substituted Models 2−5. The effects of amide (β) bond rotation on the total energies of **2**−**5** (*Group 2A*) are shown in Figure 1. All energy profiles show energy maxima at C2−N2−C1′−C2′ torsion angles of 90° and −90°, and minima at 0° and 180°. In three cases, rotating α from an *anti* to *syn* conformation displaces the curve to higher energy, with more pronounced displacements observed for the β-*cis* and β-*trans* structures (*i.e.*, for C2−N2−C1′−C2′ torsion angles near 0° and 180°). The exception is β-*gluco* **3**, where the α-*syn* and α-*anti* curves nearly coincide, except in the β-*cis* region (C2−N2−C1′−C2′ torsions near 0°). Within the complete data set, the global energy minimum is exhibited by **2** (α-*gluco*) in the α-*anti*/β-*trans* form, and the energies plotted in all curves are relative to this global minimum.

Energy differences between β-*cis* and β-*trans* forms vary with ring configuration. For α-*anti* geometries, the β-*trans* conformation is more stable than the β-*cis* by 0.4−5.0 kcal. This trend is maintained when α is rotated into a *syn* geometry, except for α-*allo* **4**, where β-*cis* appears more stable than β-*trans* (see filled symbols in Figure 1C).

In contrast to energy profiles obtained on **1**, energy barriers to amide (β) bond rotation depend on α. In general, these barriers are smaller for α-*syn* than for α-*anti* forms, especially for α-*allo* **4**.

The effects of rotating the C2−N2 (α) bond in **2**−**5** (*Group 2B* calculations) on their total energies are shown in Figure S2 (Supporting Information) for both the β-*cis* and β-*trans* geometries. These plots are less well behaved compared to those in Figure 1. For **2**, **4** and **5** in their more stable β-*trans* conformations, α-*anti* geometries are lower in energy than α-*syn*, although the overall shapes of the curves and the α-*syn*/α-*anti* energy differences vary with structure. For example, a well-defined energy minimum is observed for α-*allo* **4** (β-*trans*) at α-*anti* (H2−C2−N2−H torsion of 180°), the overall curve is symmetric about 0°, and the energy difference between α-*syn* and α-*anti* is ∼16 kcal/mol (Figure S2, D). In contrast, a flatter α-*syn* region is found for α-*gluco* **2** (β-*cis*), the overall curve is asymmetric about 0°, and the energy difference between α-*syn* and α-*anti* is much smaller (6−7 kcal/mol) (Figure S2, A). The β-*gluco* **3** (β-*trans*) configuration shows anomalous behavior, with α-*syn* forms more stable than α-*anti* by 2−3 kcal/mol (Figure S2, B). This behavior remains unexplained but may be due to differential H-bonding interactions between the *N*-acetyl side-chain in α-*syn* geometries that provide additional stabilization in these forms. This finding appears at odds with interpretations of $^{3}J_{H2,NH}$ values in structures such as β-GlcNAc that imply highly favored 180° torsions for α[11] and suggests that β-*gluco* isomers may have a greater propensity to assume α-*syn* geometries than the other three isomers. Interestingly, β-*gluco* structures are common constituents in biologically important oligosaccharides in glycoproteins.

Within the complete series, α-*gluco* (β-*trans*/α-*anti*) (**2**) is the lowest energy configuration, and all other energies are referenced to this state. Amide bond conformation can affect the shapes of these energy curves significantly, more noticeably for α-*allo* (**4**) and β-*gluco* (**3**), which presumably reflects

differences in steric and other intramolecular interactions between the ring and the side-chain in the two amide conformations.

C. Implications of Energetics Results for 1−5. The DFT-derived energetics results obtained on model structures **1**−**5** show that the effect of rotation of the C2−N2 bond of 2-acetamido-2-deoxy-aldohexopyranosyl rings on total energy depends on relative configuration at C1 and C3. In addition, conformational behavior about the C2−N2 and N2−C1′ (amide) bonds is correlated, that is, the two conformational domains are interdependent energetically. Given these overlapping dependencies of side-chain *N*-acetyl conformation on saccharide structure, experimental assessment in solution using multiple, redundant *J*-couplings is likely to prove beneficial compared to the current single *J*-coupling ($^3J_{H2,NH}$) approach. With this consideration in mind, seven new Karplus equations, five for α and two for β, were developed for use in conjunction with that for $^3J_{H2,NH}$, as described below.

D. $^3J_{H2,NH}$ and $^3J_{H2,C1'}$ Spin-Couplings. $^3J_{H2,NH}$ values have been commonly measured to evaluate conformation about the flexible C2−N2 (α) bond in 2-acetamido-2-deoxy-aldohexopyranosides in aqueous and nonaqueous solution.[10,11] In the present work, the effects of ring configuration and amide bond conformation on the $^3J_{H2,NH}$ Karplus curve were investigated using **2**−**5** as model structures (Figure 2) for comparison to this prior work. While the effects of ring configuration at C1 and C3 were found to be relatively small, amide conformation influences curve amplitude appreciably (Figure 2C). Equations 1a and 1b were, therefore, formulated to treat these two cases:

$$^3J_{H2,NH} = 5.99 - 0.59\cos\alpha + 6.11\cos(2\alpha) + 0.10\sin\alpha + 0.12\sin(2\alpha) \quad \beta\text{-}cis;\ \text{rms } 0.44 \qquad (1a)$$

$$^3J_{H2,NH} = 5.08 - 0.83\cos\alpha + 5.02\cos(2\alpha) + 0.03\sin\alpha + 0.06\sin(2\alpha) \quad \beta\text{-}trans;\ \text{rms } 0.45 \qquad (1b)$$

Recently, new $^3J_{H2,NH}$ Karplus equations have been reported for α- and β-GlcNAc anomers.[11] The shapes of the curves derived from these new equations and that for the curve derived from eq 1b are similar (Figure S3, Supporting Information), but curve amplitudes differ. The curve derived from eq 1b more closely mimics the α-GlcNAc curve,[11] with the largest deviation (∼1 Hz) found at 180°. The β-GlcNAc curve[11] deviates from that for eq 1b by ∼1 Hz at both 0° and 180°. Since contributions made by *allo* configurations affect curve amplitude considerably (Figure 2), a third $^3J_{H2,NH}$ equation was derived by fitting data from **2** and **3** only (eq 1c). This treatment gave a Karplus curve in better agreement with those reported by Mobli and Almond[11] (Figure S3, Supporting Information). The GlcNAc anomers displayed similar coupling behaviors in the present work, and thus only one generalized GlcNAc equation was developed.

$$^3J_{H2,NH} = 5.18 - 1.17\cos\alpha + 4.77\cos(2\alpha) - 0.22\sin\alpha + 0.18\sin(2\alpha) \quad \text{rms } 0.37 \qquad (1c)$$

Like $^3J_{H2,NH}$, the vicinal three-bond $^3J_{H2,C1'}$ spin-coupling is sensitive to rotation about α (Figure 3). Data obtained on the *gluco* and *allo* structures nearly coincide, and only a small

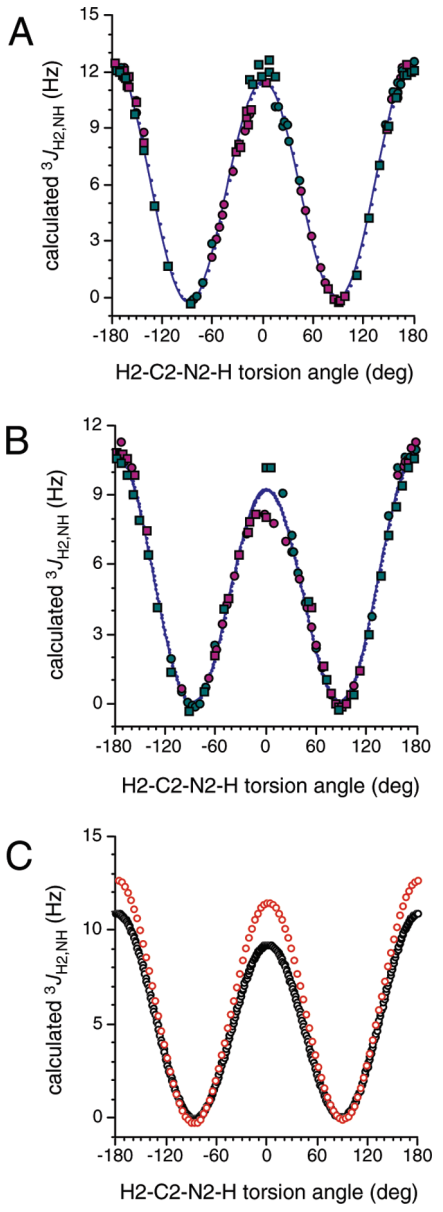

FIGURE 2. Calculated Karplus curves for $^3J_{H2,NH}$ in *β-cis* (A) and *β-trans* (B) conformations; red squares, α-*gluco* **2**; red circles, β-*gluco* **3**; green squares, α-*allo* **4**; green circles, β-*allo* **5**. (C) Comparison of the fitted $^3J_{H2,NH}$ curves for the *β-cis* (red) and *β-trans* (black) conformations, showing deviations at the maxima.

dependence on amide conformation was observed (Figure 3C). Two equations for *β-cis* and *β-trans* conformations were derived:

$$^3J_{H2,C1'} = 3.19 - 2.12\cos\alpha + 3.3\cos(2\alpha) - 0.02\sin\alpha + 0.06\sin(2\alpha) \quad \beta\text{-}cis;\ \text{rms } 0.26 \qquad (2a)$$

$$^3J_{H2,C1'} = 3.11 - 2.02\cos\alpha + 2.88\cos(2\alpha) - 0.04\sin\alpha + 0.05\sin(2\alpha) \quad \beta\text{-}trans;\ \text{rms } 0.25 \qquad (2b)$$

$^3J_{H2,C1'}$ values differ significantly at H2−C2−N2−C1′ torsion angles of 0° and 180°, with the latter coupling (∼8.5 Hz) much greater than the former (∼4 Hz). In contrast, $^3J_{H2,NH}$

spin-couplings at 0° and 180° have comparable magnitudes (~10 and ~12 Hz, respectively; Figure 2).

E. $^3J_{C1,NH}$ and $^3J_{C3,NH}$ Spin-Couplings. The two vicinal $^{13}C-^1H$ couplings involving C1 and C3 are sensitive to rotation about α. The dependency of $^3J_{C1,NH}$ is shown in Figure 4. As found for $^3J_{H2,C1'}$ (Figure 3), the *gluco* and *allo* data are virtually superimposable, and a small dependence on amide conformation is observed.

Two Karplus equations for the treatment of $^3J_{C1',NH}$ were derived from these data:

$$^3J_{C1,NH} = 3.62 - 1.32\cos\alpha + 4.13\cos(2\alpha) + 0.20\sin\alpha - 0.46\sin(2\alpha) \quad \beta\text{-}cis;\ \text{rms } 0.34 \qquad (3a)$$

$$^3J_{C1,NH} = 2.94 - 1.00\cos\alpha + 3.48\cos(2\alpha) + 0.12\sin\alpha - 0.27\sin(2\alpha) \quad \beta\text{-}trans;\ \text{rms } 0.49 \qquad (3b)$$

Karplus curves for $^3J_{C3,NH}$ are shown in Figure 5. Overall amplitudes for $^3J_{C3,NH}$ are smaller than observed for $^3J_{C1,NH}$ (Figure 4), presumably reflecting the different electronegative substitution patterns on the coupled carbon (anomeric C1 vs nonanomeric C3). Two equations were derived for the *β-cis* and *β-trans* amides:

$$^3J_{C3,NH} = 3.14 - 0.78\cos\alpha + 3.47\cos(2\alpha) - 0.16\sin\alpha + 0.37\sin(2\alpha) \quad \beta\text{-}cis;\ \text{rms } 0.33 \qquad (4a)$$

$$^3J_{C3,NH} = 2.57 - 0.61\cos\alpha + 2.92\cos(2\alpha) - 0.09\sin\alpha + 0.27\sin(2\alpha) \quad \beta\text{-}trans;\ \text{rms } 0.44 \qquad (4b)$$

F. $^3J_{C1,C1'}$ and $^3J_{C3,C1'}$ Spin-Couplings. Two vicinal $^{13}C-^{13}C$ spin-couplings report on conformation about α, $^3J_{C1,C1'}$ and $^3J_{C3,C1'}$, and the Karplus dependency of $^3J_{C1,C1'}$ is shown in Figure 6. While the dynamic ranges for $^3J_{HCNH}$, $^3J_{HCNC}$, and $^3J_{CCNH}$ couplings are relatively high (6−13 Hz), that for $^3J_{C1,C1'}$ is modest, with a maximum coupling of ~5 Hz observed at a C1−C2−N2−C1′ torsion angle of 180°. As found for $^3J_{H2,C1'}$ (Figure 3), calculated couplings at 180° are considerably larger than those at 0°, the latter ranging from 1 to 1.5 Hz. The effect of ring configuration is negligible, but a small shift of the curve is discernible upon conversion of *cis* to *trans* amide (Figure 6C). Two Karplus eqs 5a and 5b were parametrized from these data:

$$^3J_{C1,C1'} = 1.37 - 1.52\cos\alpha + 1.62\cos(2\alpha) + 0.10\sin\alpha - 0.15\sin(2\alpha) \quad \beta\text{-}cis;\ \text{rms } 0.41 \qquad (5a)$$

$$^3J_{C1,C1'} = 1.27 - 1.31\cos\alpha + 1.36\cos(2\alpha) + 0.12\sin\alpha - 0.07\sin(2\alpha) \quad \beta\text{-}trans;\ \text{rms } 0.30 \qquad (5b)$$

The dependence of $^3J_{C3,C1'}$ on the C3−C2−N2−C1′ torsion angle is shown in Figure 7. These curves are similar to those found for $^3J_{C1,C1'}$; the slightly reduced amplitude at the C3−C2−N2−C1′ torsion of 180° relative to that observed for $^3J_{C1,C1'}$ mimics those observed between $^3J_{C1,NH}$ and $^3J_{C3,NH}$ (Figures 4 and 5). Equations 6a and 6b were parametrized for the *cis* and *trans* amides, respectively; while considerable data scatter prevented a reliable appraisal of the effect of ring configuration, an effect might be present for C3−C2−N2−C1′ torsions near 0° in the *β-trans* amide (Figure 7B).

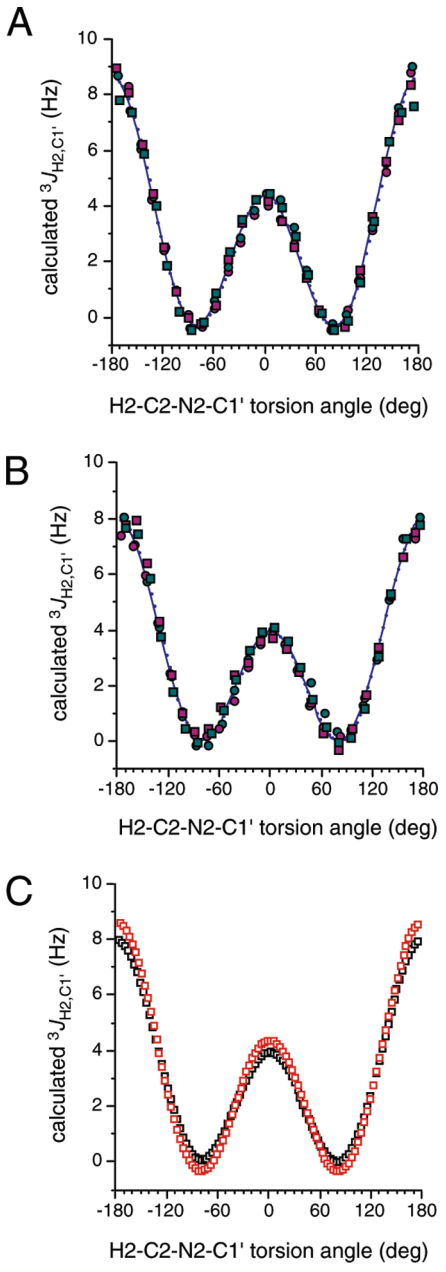

FIGURE 3. Calculated Karplus curves for $^3J_{H2,C1'}$ in *β-cis* (A) and *β-trans* (B) conformations. In A and B: red squares, α-*gluco* **2**; red circles, *β-gluco* **3**; green squares, α-*allo* **4**; green circles, *β-allo* **5**. (C) Comparison of the fitted $^3J_{H2,C1'}$ curves for the *β-cis* (red symbols) and *β-trans* (black symbols) conformations.

$$^3J_{C3,C1'} = 1.12 - 0.97\cos\alpha + 1.35\cos(2\alpha) - 0.16\sin\alpha + 0.04\sin(2\alpha) \quad \beta\text{-}cis;\ \text{rms } 0.36 \qquad (6a)$$

$$^3J_{C3,C1'} = 1.11 - 0.87\cos\alpha + 1.15\cos(2\alpha) - 0.09\sin\alpha + 0.08\sin(2\alpha) \quad \beta\text{-}trans;\ \text{rms } 0.27 \qquad (6b)$$

G. $^3J_{NH,C2'}$ and $^3J_{C2,C2'}$ Spin-Couplings. $^3J_{NH,C2'}$ and $^3J_{C2,C2'}$ in the *N*-acetyl side-chain hold the potential for distinguishing between *cis* and *trans* amide conformations. The

dependence of $^3J_{NH,C2'}$ on amide conformation is shown in Figure 8.

This coupling shows a small dependence on ring configuration (possibly at H2−N2−C1′−C2′ torsions of 180°), but essentially no dependence on α. A difference of ~3 Hz is observed between the *cis* and *trans* amides, with the latter giving the greater coupling. Parametrization gave the following generalized Karplus eq 7:

$$^3J_{NH,C2'} = 1.62 - 2.59\cos\beta + 1.29\cos(2\beta) + 0.67\cos(3\beta) + 0.02\sin\beta - 0.02\sin(2\beta) + 0.003\sin(3\beta) \quad \text{rms } 0.39 \qquad (7)$$

Unlike $^3J_{NH,C2'}$, $^3J_{C2,C2'}$ is affected by both ring configuration and conformation about α (Figure 9). The former appears greater in the α-*syn* form, notably for C2−N2−C1′−C2′ torsions near 180°. However, since the effect of α conformation is considerably greater than that of ring configuration, only two generalized eqs 8a and 8b were parametrized:

$$^3J_{C2,C2'} = 0.84 - 2.03\cos\beta + 0.60\cos(2\beta) + 0.13\cos(3\beta) + 0.04\sin\beta - 0.02\sin(2\beta) - 0.002\sin(3\beta) \quad \alpha\text{-}syn;\ \text{rms } 0.28 \qquad (8a)$$

$$^3J_{C2,C2'} = 0.39 - 1.03\cos\beta + 0.36\cos(2\beta) + 0.25\cos(3\beta) - 0.01\sin\beta + 0.02\sin(2\beta) - 0.004\sin(3\beta) \quad \alpha\text{-}anti;\ \text{rms } 0.10 \qquad (8b)$$

H. Comparison of Related *J*-Couplings in the Exocyclic *N*-Acetyl Fragment of Saccharides and in Proteins. Some *J*-couplings within saccharide *N*-acetyl side-chains involve coupling pathways related structurally to those found along protein backbones (Scheme S1, Supporting Information), and substantial efforts have been made to parametrize the latter for use in protein structure determination.[20−22] Specifically, $^3J_{H2,NH}$, $^3J_{H2,C1'}$, $^3J_{C1/C3,NH}$ and $^3J_{C1/C3,C1'}$ discussed above correspond to $^3J_{NH,H\alpha}$, $^3J_{CO,H\alpha}$, $^3J_{NH,C\beta}$ and $^3J_{CO,C\beta}$, respectively, in proteins. A discussion of these four pairs of *J*-couplings follows. The saccharide parametrizations are compared to those reported for their protein counterparts, with the aim of determining how each pair of related couplings differ with respect to their structural dependencies and whether these differences can be attributed to specific changes in pathway substitution.

The $H_\alpha-C_\alpha-N-H$ coupling pathway in proteins is related to the H2−C2−N2−H pathway in **2**−**5** (Scheme S1, Supporting Information), and several $^3J_{H\alpha,NH}$ Karplus equations have been reported for use in protein structure determination (Figure S4, Supporting Information).[20,21] The saccharide and protein curves have similar overall shapes, with the global maximum occurring at ±180° (10−11 Hz) and a local maximum occurring at 0° (6.5−9 Hz); variability appears greater at 0°. Two nearly equivalent minima are observed at ±80−90° in all curves. Overall, identical or larger couplings are predicted in the saccharide at nearly all torsion angles.

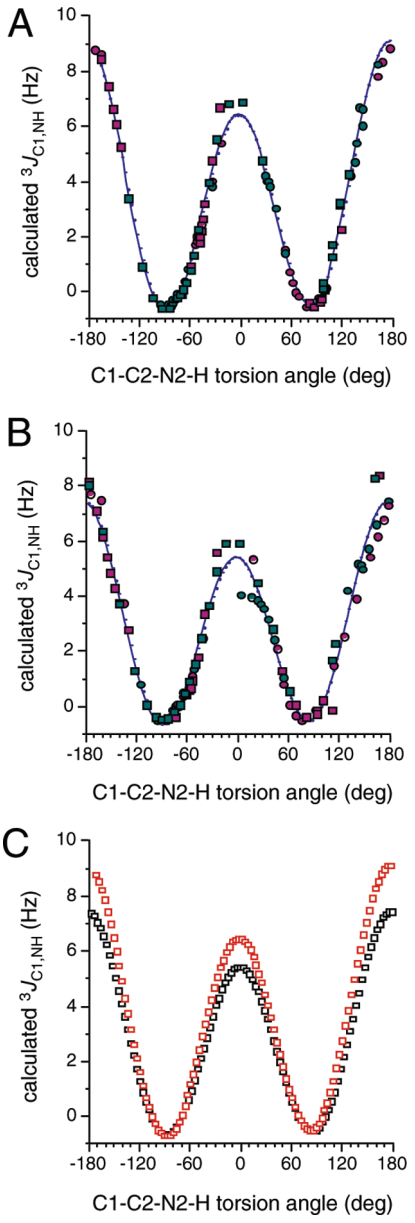

FIGURE 4. Calculated Karplus curves for $^3J_{C1,NH}$ in *β-cis* (A) and *β-trans* (B) conformations. In A and B: red squares, α-*gluco* **2**; red circles, *β-gluco* **3**; green squares, α-*allo* **4**; green circles, *β-allo* **5**. (C) Comparison of the fitted $^3J_{C1,NH}$ curves for the *β-cis* (red symbols) and *β-trans* (black symbols) conformations.

The $^3J_{H2,C1'}$ spin-coupling in **2**−**5** is related to $^3J_{H\alpha,CO}$ in proteins (Scheme S1, Supporting Information), and Karplus curves for these *J*-couplings are shown in Figure S5 (Supporting Information). A modest degree of variability is observed at the maxima: 7−8 Hz for the global maximum at ±180° and 2.8−3.9 Hz for the local maximum at 0°. The protein curves give uniformly smaller couplings at both maxima relative to the saccharide curve.

The C1/C3−C2−N2−H coupling pathways in **2**−**5** are related to the $C_\beta-C_\alpha-N-H$ pathway in proteins (Scheme S1, Supporting Information), and $^3J_{C\beta,NH}$ behavior[20−22] is compared to those of $^3J_{C1,NH}$ and $^3J_{C3,NH}$ in Figure S6 (Supporting Information). Compared to the $^3J_{H2,C1'}/^3J_{H\alpha,CO}$ curves shown in Figure S5, significant variability is observed at

(20) Vögeli, B.; Ying, J.; Grishaev, A.; Bax, A. *J. Am. Chem. Soc.* **2007**, *129*, 9377–9385.
(21) Case, D. A.; Scheurer, C.; Brüschweiler, R. *J. Am. Chem. Soc.* **2007**, *129*, 9377–9385.
(22) Hu, J.-S.; Bax, A. *J. Am. Chem. Soc.* **1997**, *119*, 6360–6368.

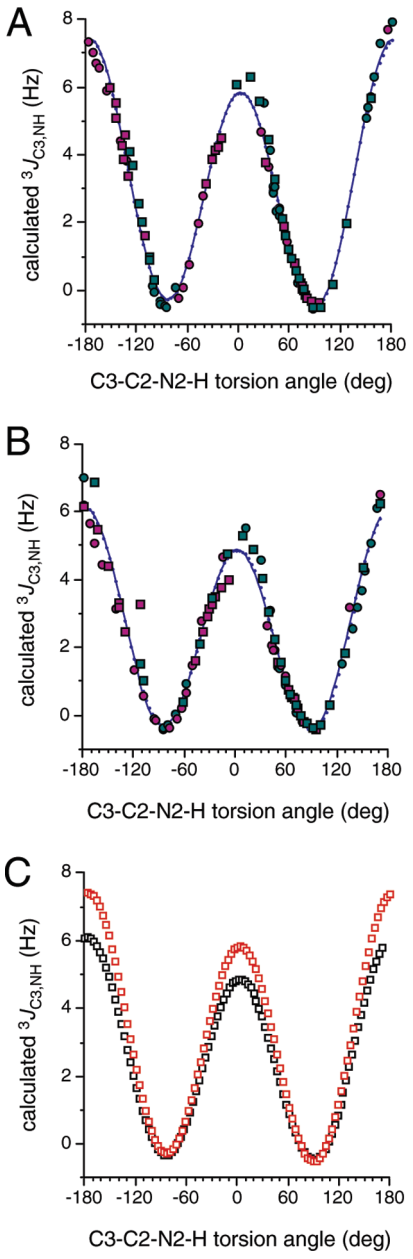

FIGURE 5. Calculated Karplus curves for $^3J_{C3,NH}$ in *β-cis* (A) and *β-trans* (B) conformations. In A and B: red squares, α-*gluco* **2**; red circles, *β-gluco* **3**; green squares, α-*allo* **4**; green circles, *β-allo* **5**. (C) Comparison of the fitted $^3J_{C3,NH}$ curves for the *β-cis* (red symbols) and *β-trans* (black symbols) conformations.

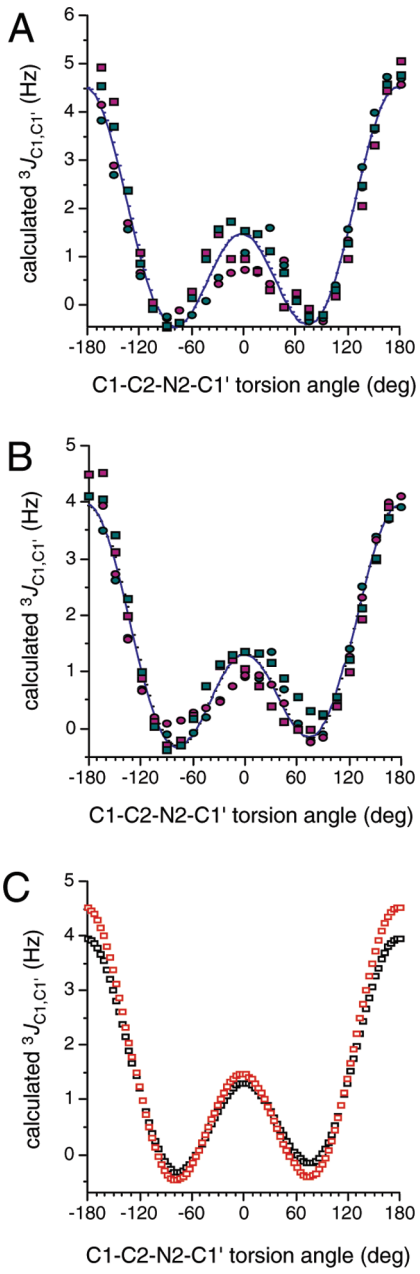

FIGURE 6. (A) Calculated Karplus curves for $^3J_{C1,C1'}$ in *β-cis* (A) and *β-trans* (B) conformations. In A and B: red squares, α-*gluco* **2**; red circles, *β-gluco* **3**; green squares, α-*allo* **4**; green circles, *β-allo* **5**. (C) Comparison of the fitted $^3J_{C1,C1'}$ curves for the *β-cis* (red symbols) and *β-trans* (black symbols) conformations.

both maxima: 3.1−7.4 Hz at ±180° and 2.3−5.3 Hz at 0°. Overall curve shapes are similar, but amplitude is significantly diminished for $^3J_{C\beta,NH}$, presumably due to the different intervening carbons along the two pathways (C_α substituted with hydrogen and a carboxyl group versus C2 bound to hydrogen and the anomeric carbon). The "internal" carboxyl effect reduces curve amplitude, while increasing the number of electronegative substituents on the terminal coupled carbon increases amplitudes. In addition to these substituent effects, N−H bond lengths in the protein and saccharide pathways may also differ, which may influence $^3J_{CCNH}$ values.

Proteins contain a $^3J_{CO,C\beta}$ coupling[21,22] related to the saccharide $^3J_{C1,C1'}$ and $^3J_{C3,C1'}$ values (Scheme S1, Supporting Information), and their behaviors are compared in Figure S7 (Supporting Information). The ensemble of curves have conserved shapes, but their amplitudes are considerably reduced relative to those observed in the other three coupling pairs. Variability at 180° (3.5−4.0 Hz) is similar to that found at 0° (0.9−2.1 Hz).

The above comparisons suggest that pathway structural differences in saccharides and proteins, while apparently small, are nevertheless sufficient to produce observable differences in coupling behaviors. The C_α carbon of proteins (with H, C_β and CO substituents) and the C2 carbon of aminosugars (with H2, C1 and C3 substituents) are not structurally

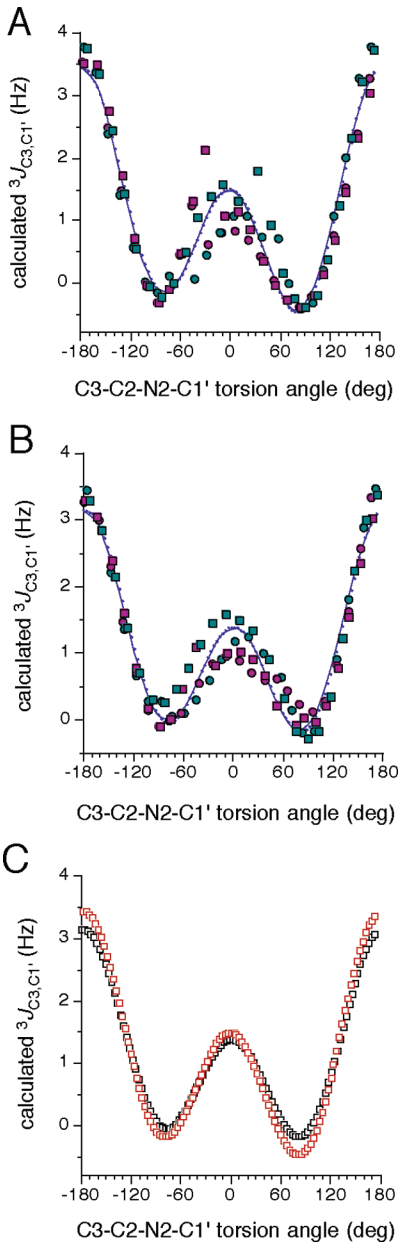

FIGURE 7. Calculated Karplus curves for $^3J_{C3,C1'}$ in *β-cis* (A) and *β-trans* conformations (B). In A and B: red squares, α-*gluco* **2**; red circles, *β-gluco* **3**; green squares, α-*allo* **4**; green circles, *β-allo* **5**. (C) Comparison of the fitted $^3J_{C3,C1'}$ curves for the *β-cis* (red symbols) and *β-trans* (black symbols) conformations.

equivalent (a net effect of exchanging C1 and CO), and all of the couplings examined are subject to an "internal" substitution effect since all involve C2/C_α in the coupling pathway. In addition, both "internal" and "terminal" substitution effects are probably operative for $^3J_{C1/C3,NH}$/$^3J_{C\beta,NH}$ and $^3J_{C1/C3,C1'}$/$^3J_{CO,C\beta}$, resulting in a greater likelihood of differences between these coupling pairs. Thus, the existence of "internal" and/or "terminal" substitution effects on $^3J_{HH}$, $^3J_{CH}$ and $^3J_{CC}$ obviates the use of protein *J*-coupling parametrizations to interpret related *J*-couplings in saccharides; separate parametrizations for each system appear to be required.

I. Effect of Solvation on DFT-Calculated *J*-Couplings. The parametrization of eqs 1−8 was achieved using DFT calculations in which both the geometry optimization (*G*-component) and *J*-coupling calculations (*J*-component) were conducted under *in vacuo* conditions. Given the potential influence of solvent water on these calculations, a limited study was conducted on *β-gluco* **3** in which solvent effects from water on both the *G*- and *J*-components were investigated. These calculations yielded four data sets: G_{vac}/J_{vac}; G_{sol}/J_{vac}; G_{vac}/J_{sol}; G_{sol}/J_{sol}. The G_{vac}/J_{vac} data encompass the *Group 2B* calculations used to parametrize eqs 1−8.

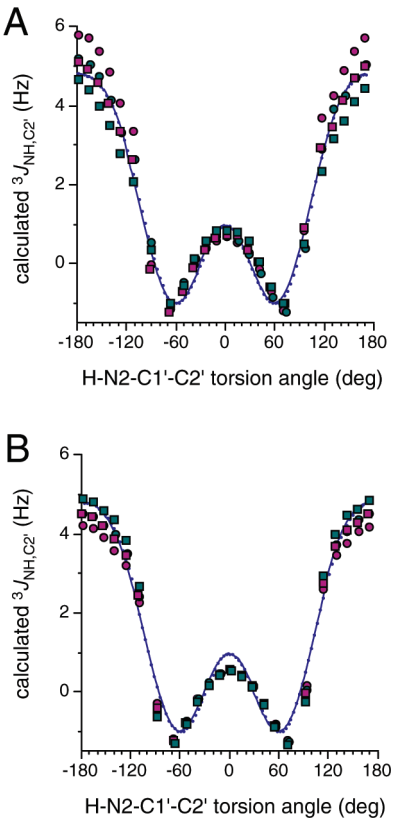

FIGURE 8. Calculated Karplus curves for $^3J_{NH,C2'}$ in the α-*syn* (A) and α-*anti* (B) conformation. In A and B: red squares, α-*gluco* **2**; red circles, *β-gluco* **3**; green squares, α-*allo* **4**; green circles, *β-allo*. The fitted curves in A and B describe eq 7.

Data obtained on four representative *J*-couplings ($^3J_{H2,NH}$, $^3J_{H2,C1'}$, $^3J_{C1,NH}$, $^3J_{C1,C1'}$) are shown in Figure S8 (Supporting Information). Each plot contains data points from the four data sets superimposed on the appropriate fitted Karplus equation derived from the $G_{vac}J_{vac}$ data. Data from the four data sets are in good agreement with the fitted curve in each case, showing that inclusion of solvent water in either or both components of the calculations does not affect the calculated *J*-couplings significantly. Data for $^3J_{C1,C1'}$ show some deviation from the fitted curve at C1−C2−N2−C1′ torsion angles between −60° and −120°, but this deviation is caused by inclusion of data from structures **2**, **4** and **5** in the calculation of the fitted curve (see Figure 6), not by solvation effects.

The results shown in Figure S8 suggest that the *in vacuo* data used in the formulation of eqs 1−8 provide a reliable appraisal of *J*-coupling behavior in solution. It should be noted, however, that the methodology used to introduce the effects of solvent water does not involve explicit water but rather a somewhat artificial dielectric continuum, and thus the apparently good agreement between *in vacuo* and solvated

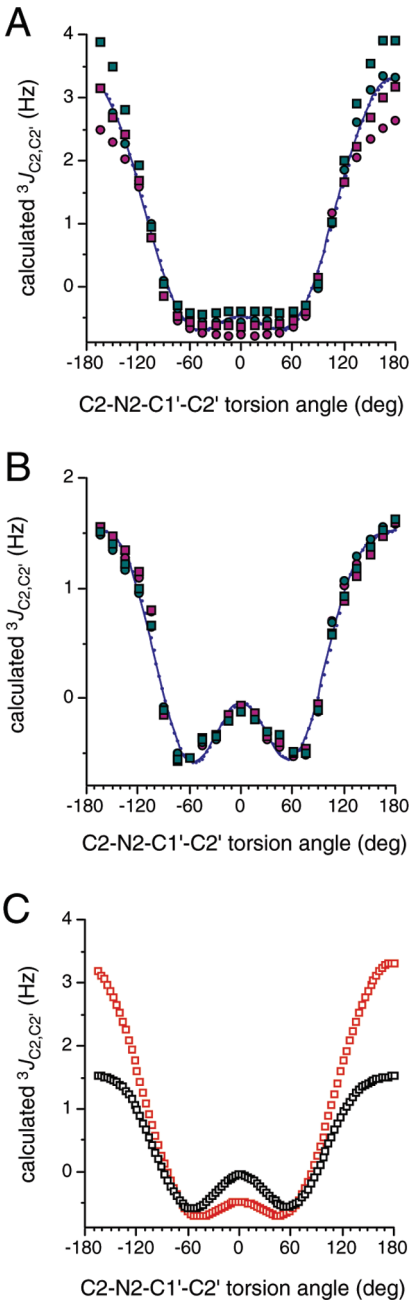

FIGURE 9. Calculated Karplus curves for $^3J_{C2,C2'}$ in the α-*syn* (A) and α-*anti* (B) conformations. In A and B: red squares, α-*gluco* **2**; red circles, *β*-*gluco* **3**; green squares, α-*allo* **4**; green circles, *β*-*allo* **5**. (C) Comparison of the fitted $^3J_{C2,C2'}$ curves for the α-*syn* (red symbols) and α-*anti* (black symbols) conformations.

data may be due largely to an inability of the current calculational methodology to accurately mimic water−solute interactions in solution.

J. Experimental *J*-Couplings in Methyl 2-Acetamido-2-deoxy-α-D-glucopyranoside 6. ^{13}C-Labeled **6** (Scheme 5) was prepared[7,23] as a model system to measure and treat the ensemble of experimental *J*-couplings within its constituent *N*-acetyl side-chain. Experimental *J*-couplings in **6** (Scheme 5) involving the NH proton were measured in DMSO-d_6 solvent,

SCHEME 5

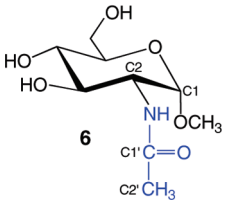

$^3J_{H2,NH}$ = 8.3 Hz (DMSO-d_6)
$^3J_{H2,C1'}$ = 3.1 Hz (D_2O)
$^3J_{C1,NH}$ = 0 Hz (DMSO-d_6)
$^3J_{C3,NH}$ = 1.3 Hz (DMSO-d_6)
$^3J_{C1,C1'}$ = 1.1 Hz (D_2O)
$^3J_{C3,C1'}$ = 1.5 Hz (D_2O)
$^3J_{C2,C2'}$ = 1.6 Hz (D_2O)

whereas all others were measured in ^2H_2O; their values are shown in Scheme 5.[24] The experimental couplings were treated as described previously for interpreting trans-glycoside *J*-couplings in oligosaccharides.[25,26] An ensemble of *J*-couplings sensitive to the same torsion angle (in this case, those sensitive to α; Scheme 5) is first calculated over the full 360° range of torsion angles (1° increments) using the parametrized Karplus equation derived for each *J*-coupling. This data set is then used to calculate an rms error at each torsion angle using the experimental *J*-couplings, and these latter data are plotted to visualize those torsions giving low rms errors. In the present case, four groups of *J*-couplings in Scheme 5 were examined: Group 1, only $^3J_{H2,NH}$; Group 2, only $^3J_{C1,NH}$ and $^3J_{C3,NH}$; Group 3, only $^3J_{H2,C1'}$, $^3J_{C1,C1'}$ and $^3J_{C3,C1'}$; and Group 4, all six *J*-couplings. The results of this treatment are plotted in Figure 10. This analysis considers only whether a single-state model is sufficient to fit the experimental *J*-coupling data satisfactorily; it does not eliminate two- or multiple-state models as alternate possibilities. In the present case, rotation about α could obey a two-state *syn*-*anti* model, but herein only the single-state case is considered; more complete treatments will follow in future work.

Inspection of the Group 1 plot (Figure 10) shows two regions with very low rms errors: ±20° (α-*syn*) and ±150° (α-*anti*). Thus, $^3J_{H2,NH}$ alone cannot be used to distinguish between these two single-state models. This situation derives from the very similar $^3J_{H2,NH}$ magnitudes at H2−C2−N2−H torsion angles of 0° and 180° (Figure 2). Indeed, even two-state α-*syn*/α-*anti* models with widely different populations of both forms in solution cannot be distinguished on the basis of $^3J_{H2,NH}$ alone.

At the other extreme in the fitting treatment, Group 4 yields the lowest rms error near +160°, and a local minimum at −30°. This treatment supports a single-state model for α in which the *anti* conformation predominates, although some contribution from α-*syn* is possible in solution.

Different combinations of the *J*-couplings give different rms error plots. For example, treatment of only $^3J_{C1,NH}$ and $^3J_{C3,NH}$ (Group 2, Figure 10) gives a result similar to that obtained from Group 4, with a global minimum at ∼180°

(23) Zhu, Y.; Pan, Q.; Thibaudeau, C.; Zhao, S.; Carmichael, I.; Serianni, A. S. *J. Org. Chem.* **2006**, *71*, 466–479.

(24) Three of the six *J*-couplings involving the solvent-exchangeable NH proton were measured in DMSO-d_6 to avoid complications arising from solvent exchange in ^2H_2O. Some error in the rms error analysis may result from the use of two groups of *J*-couplings measured in two different solvents, but this error is expected to be negligible in the present single-state analysis of the data. Future more quantitative analyses will likely use either ^2H_2O solvent at room temperature containing a small amount of ^1H_2O to allow detection of weak NH signals (see refs 23 and 28), or a mixed acetone-d_6/^2H_2O solvent at low temperature to suppress solvent exchange (see ref 28), to permit measurement of all *N*-acetyl related *J*-couplings in a single solvent.

(25) Bose, B.; Zhao, S.; Stenutz, R.; Cloran, F.; Bondo, P. B.; Bondo, G.; Hertz, B.; Carmichael, I.; Serianni, A. S. *J. Am. Chem. Soc.* **1998**, *120*, 11158–11173.

(26) Olsson, U.; Serianni, A. S.; Stenutz, R. *J. Phys. Chem. B* **2008**, *112*, 4447–4453.

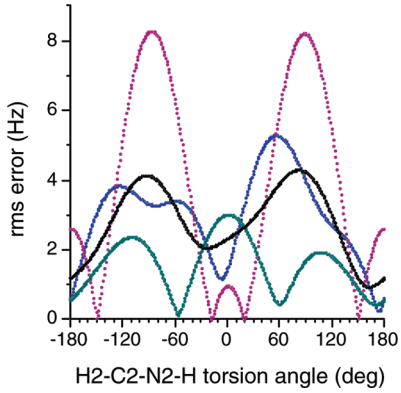

FIGURE 10. Plot of rms error versus the H2−C2−N2−H torsion angle in **6** using four different groups of *J*-couplings sensitive to α. Burgundy points = Group 1. Blue points = Group 2. Green points = Group 3. Black points = Group 4. See text for group definitions.

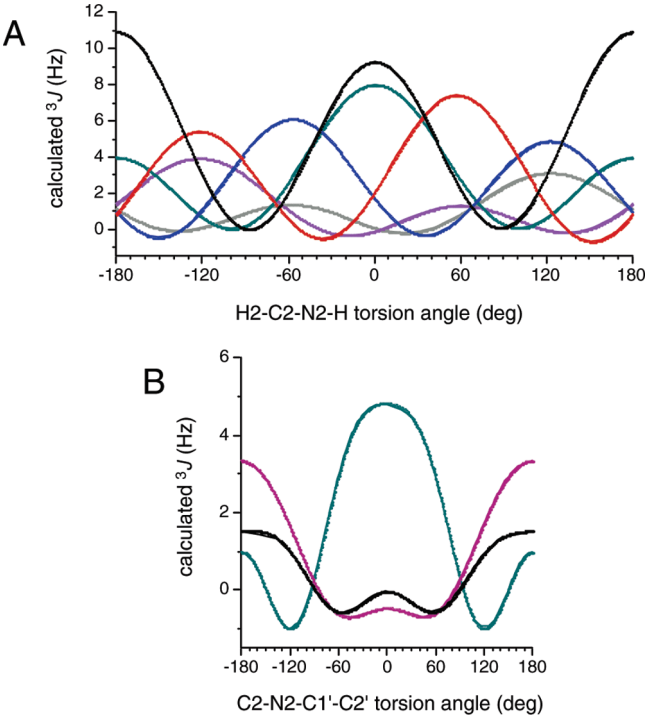

FIGURE 11. (A) Torsional dependencies for the ensemble of *J*-couplings sensitive to rotation about α (A) and *β* (B). In A, data were normalized to a common torsion angle (H2−C2−N2−H). Curves were derived from eqs 1−6 for *β-trans* conformations with appropriate phase shifting of the *x*-axis. Black = $^{3}J_{H2,NH}$; red = $^{3}J_{C1,NH}$; blue = $^{3}J_{C3,NH}$; green = $^{3}J_{H2,C1'}$; purple = $^{3}J_{C1,C1'}$; gray = $^{3}J_{C3,C1'}$. In B, data were normalized to a common torsion angle (C2−N2−C1′−C2′). Curves were derived from eqs 7 and 8 with appropriate phase shifting of the *x*-axis. Black = $^{3}J_{C2,C2'}$, α-*anti*; red = $^{3}J_{C2,C2'}$, α-*syn*; green = $^{3}J_{NH,C2'}$.

and a local minimum at ∼0°. In contrast, treatment of $^{3}J_{H2,C1'}$, $^{3}J_{C1,C1'}$ and $^{3}J_{C3,C1'}$ (Group 3) gives a global minimum near −60° and local minima near +60° and +170°. These results are caused by the different sensitivities of the individual *J*-couplings used in the fitting to changes in the H2−C2−N2−H torsion angle (see Figure 11); for example, fitting two *J*-couplings with similar H2−C2−N2−H torsion angle dependencies reduces the discriminatory power of the fit. In general, the treatment should utilize as many *J*-couplings as possible with different torsional dependencies in order to increase the reliability of the analysis.

Conclusions

This investigation describes the development of new Karplus equations for conformational analysis of the exocyclic *N*-acetyl groups of saccharides. This side-chain contains two bonds that determine its overall conformation, namely, the flexible C2−N2 bond (α) and the more rotationally restricted amide bond (*β*). Eight NMR vicinal spin−spin coupling constants have been investigated, six that report on α and two that report on *β*.

Within the α-sensitive group, $^{3}J_{H2,NH}$ has received considerable prior attention and has been used commonly to distinguish between two limiting conformations about this bond, namely, α-*syn* (H2−C2−N2−H torsion = 0°) and α-*anti* (H2−C2−N2−H torsion = 180°). However, as shown in Figure 2, the difference in $^{3}J_{H2,NH}$ values in these limiting conformations is small (1.5−2 Hz), and this relatively small dynamic range limits the ability of this coupling to distinguish between these two limiting states or between more complex conformational models. For this reason, efforts were made to develop additional α-sensitive *J*-couplings for use as complementary structural probes. In addition, *J*-couplings that involve NH protons are more challenging to measure because of the solvent exchange properties of the NH proton in aqueous solution. For this reason, access to *J*-couplings that are sensitive to α but do not involve NH sites (e.g., $^{3}J_{C1,C1'}$ and $^{3}J_{C3,C1'}$) offer some advantages, although their limited dynamic ranges in comparison to $^{3}J_{HH}$ and $^{3}J_{CH}$ reduce their effectiveness as singular conformational probes. Similar arguments have been made recently in conformational analyses of C−O bond torsions in saccharides, where detection of *J*-couplings such as $^{3}J_{HCOH}$ and $^{3}J_{CCOH}$ are hampered by hydroxyl proton exchange in aqueous solution, and inspection of complementary $^{2}J_{CCH}$ and $^{2}J_{CCC}$ can prove valuable.[27,28]

The dependencies of the six vicinal *J*-couplings on rotation about α, normalized to a common torsion angle (H2−C2−N2−H), are shown in Figure 11A. Focusing on the limiting α conformations only, it is noteworthy that the *difference* between $^{3}J_{H2,NH}$ and $^{3}J_{H2,C1'}$ values may serve as a useful qualitative probe of α, being small in α-*syn* (∼1.5 Hz) and considerably larger in α-*anti* (∼7 Hz). This difference provides more reliable information about α than using either *J*-coupling alone, since calculated differences are likely to be more accurate than calculations of the absolute values of individual *J*-couplings. The four remaining α-sensitive *J*-couplings are relatively small in both the α-*syn* and α-*anti* conformations; in α-*anti*, all four converge to a common small value, whereas in α-*syn*, two groups are observed, with the two $^{13}C-^{13}C$ couplings ($^{3}J_{C1,C1'}$ and $^{3}J_{C3,C1'}$) giving an average value of ∼0 Hz,

(27) Klepach, T. E.; Carmichael, I.; Serianni, A. S. *J. Am. Chem. Soc.* **2005**, *127*, 9781–9793.

(28) Zhao, H.; Pan, Q.; Zhang, W.; Carmichael, I.; Serianni, A. S. *J. Org. Chem.* **2007**, *72*, 7071–7082.

(29) This survey was conducted on 1311 PDB files (from the RCSB PDB database) containing a total of 7994 GlcNAc residues. Within the latter group, 917 residues contained a H2−C2−N2−H torsion angle between 60° and −60°, producing an ∼11% α-*syn* population; the remaining ∼89% is α-*trans*. With regard to amide conformation, 463 residues contained a C2−N2−C1′−C2′ torsion angle between 60° and −60°, giving an ∼6% *β-cis* population.

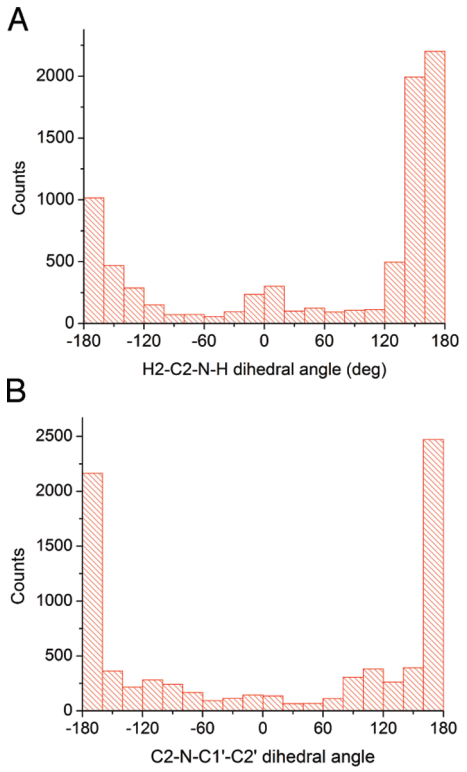

FIGURE 12. Distribution of α torsion angles (A) and C2−N2−C1′−C2′ dihedral angles (β) (B) in an ensemble of X-ray structures of GlcNAc in the PDB.[29] In B, note the predominance of β-*trans* (180°) but also the relatively continuous distribution of angles over the full 360° rotation, including the β-*cis* form (0°).

and the two $^{13}C-^{1}H$ couplings ($^{3}J_{C1,NH}$ and $^{3}J_{C3,NH}$) giving an average value of ∼2 Hz.

In simple monosaccharides such as GlcNAc and GalNAc (Scheme 1), the conformational behavior of the *N*-acetyl side-chain is likely to be simple, that is, one geometry about α highly preferred (i.e., α-*anti*), with little (or restricted) conformational averaging (i.e., essentially a single-state model). However, in more complex structural contexts, such as in oligo- and polysaccharides such as hyaluronic acid (Scheme 1), the side-chain may adopt α geometries that differ from the limiting cases due to competing intra- and intermolecular interactions, and more complex conformational models may pertain. Indeed, an examination of the protein crystallographic databases reveals a wide range of conformations about α in the GlcNAc residues of glycoproteins (Figure 12A). In these instances, access to the ensemble of *J*-couplings described herein may prove valuable in confirming the presence of nonstandard behavior in solution. For example, at H2−C2−N2−H torsions near 70°, $^{3}J_{C1,NH}$ dominates over the remaining five *J*-couplings, whereas at −70°, $^{3}J_{C3,NH}$ dominates. More complicated patterns are found at torsions of 120° and −120°.

Conformation of the amide bond in simple aminosugars such as GlcNAc is predominantly *trans*, a conclusion supported by two lines of experimental evidence. First, recent NMR investigations have demonstrated the presence of both *cis* and *trans* amides in aqueous solutions of GlcNAc and related structures, with the latter present in ∼50-fold higher concentration than the former at 42 °C.[7] Second, a survey of the protein crystallographic databases shows a preference for the *trans* amide in GlcNAc residues (Figure 12B). These data, however, also reveal the presence of a considerable *cis* amide population, as well as a range of geometries between these two limiting conformations. While ^{1}H and ^{13}C chemical shifts can be used to distinguish between *cis* and *trans* amides in solution,[7] the present findings show that two vicinal *J*-couplings within the *N*-acetyl fragment are also sensitive to this structural change (Figure 11B). Their dependencies are complementary, thus allowing them to be used in concert to confirm amide conformation. For example, the absolute *difference* between $^{3}J_{C2,C2'}$ and $^{3}J_{NH,C2'}$ is predicted to be much greater in *cis* amides (∼5 Hz) than in *trans* amides (∼0.5 Hz), especially for the more likely α-*anti* conformations (Figure 11B).

The present work is a prerequisite to experimental *J*-coupling investigations of saccharide *N*-acetyl side-chain conformation in different structural contexts in solution. To this end, complementary experimental work is underway to apply these equations collectively to examine *N*-acetyl conformation in ^{13}C-labeled methyl glycosides of GlcNAc and AllNAc, that is, in experimental compounds that replicate model structures **2**−**5** used in the present theoretical work to parametrize eqs 1−8. The results of this work will be discussed in a future report.

Acknowledgment. This work was supported by a grant (to A.S.) from the National Institutes of Health (GM059239). The Notre Dame Radiation Laboratory is supported by the Office of Basic Energy Sciences of the United States Department of Energy. This is Document No. NDRL-4838 from the Notre Dame Radiation Laboratory.

Supporting Information Available: Description of the Karplus equation fitting procedure; dependence of total energy on amide bond rotation in **1**; effect of rotation of α on total energies of **2**−**5**; comparison of $^{3}J_{H2,NH}$ reported for α-GlcNAc and β-GlcNAc (ref 11) to the Karplus curves described by eqs 1b and 1c; comparison of calculated $^{3}J_{H2,NH}$ Karplus curves to that for $^{3}J_{NH,H\alpha}$ in proteins; comparison of calculated $^{3}J_{H2,C1'}$ Karplus curves to that for $^{3}J_{H\alpha,CO}$ in proteins; comparison of calculated $^{3}J_{C1,NH}$ and $^{3}J_{C3,NH}$ Karplus curves to that for $^{3}J_{NH,C\beta}$ in proteins; comparison of calculated $^{3}J_{C1,C1'}$ and $^{3}J_{C3,C1'}$ Karplus curves to that for $^{3}J_{CO,C\beta}$ in proteins; effect of solvation on the geometric optimization and *J*-coupling components of DFT *J*-coupling calculations; related *J*-coupling pathways in the exocyclic *N*-acetyl fragment of saccharides and in proteins; Cartesian coordinates for representative DFT structures **1**−**5**; complete ref 12. This material is available free of charge via the Internet at http://pubs.acs.org.